Pergamon

Int. J. Heat Mass Transfer. Vol. 41, No. 16, pp. 2437–2454, 1998
© 1998 Elsevier Science Ltd. All rights reserved
Printed in Great Britain
0017–9310/98 \$19.00+0.00

PII: S0017–9310(97)00367–0

Laminar natural convection in a laterally heated and upper cooled vertical cylindrical enclosure

A. LEMEMBRE and J.-P. PETIT
Laboratoire E.M2.C., C.N.R.S. et Ecole Centrale des Arts et Manufactures,
92295 Châtenay-Malabry, France

(*Received* 6 *December* 1996 *and in final form* 10 *November* 1997)

Abstract—Numerical simulation of laminar natural convection in a vertical cylinder is proposed. The cylinder is insulated at the bottom, laterally heated at a uniform heat flux density and cooled at the same flux at the top surface. The influence of the characteristic parameters of the problem on the steady-state solution is analysed ($10^2 \leqslant Ra \leqslant 10^6$; $0.7 \leqslant Pr \leqslant 92.5$; $1/5 \leqslant Al \leqslant 2$). The fluid transient behaviour is also investigated. It is found that the stationary convective heat transfer is more important at the top surface for $1/5 \leqslant Al \leqslant 1/2$ and is explicitly independent of the Prandtl number. The steady-state flow presents a single roll pattern in all cases. On the other hand, in the transient phase a time-limited two-roll flow is predicted when $Al \leqslant 1/3$. © 1998 Elsevier Science Ltd. All rights reserved.

1. INTRODUCTION

If natural flows in rectangular boxes have been intensively investigated, there are very few studies of natural convection in vertical cylindrical enclosures. However, these geometries are of great fundamental and practice interest to understand, for instance, convection phenomena in hydrocarbon storage tanks. Most studies in vertical cylinders deal with the Rayleigh–Bénard problem, where a fluid layer is heated from below, cooled at its upper surface and generally laterally insulated. In this configuration Neumann [1] used stability analysis to determine the critical Rayleigh number beyond which the axisymmetric modes are not stable. Figliola [2] has performed experiments and flow visualizations of the convection of a high Prandtl number fluid. In the same way, Guthmann *et al.* [3] found interesting experimental flow structures in large-aspect-ratio cavities. Liang *et al.* [4] demonstrated the influence of the temperature field initialization on the possibility of obtaining two steady-state solutions, one with upflow and the other with downflow at the centre of the cell. The work on the laterally heated fluid layer is much more limited. We can cite, for instance, the analysis of Huang *et al.* [5] who have simulated buoyancy-driven flows in a container heated from above and the side.

Our paper concerns the numerical simulation of the flow which occurs in a vertical cylinder which is insulated at the bottom, laterally heated at a uniform heat flux density and cooled with the same flux on the ceiling. The main objective is, on the one hand, to understand the influence of the Rayleigh number, the aspect ratio and the Prandtl number on the steady-state solutions, and, on the other hand, to examine the fluid transient behaviour.

2. MATHEMATICAL MODEL

The geometry of the problem is presented in Fig. 1. The flow is assumed to be laminar and two-dimensional. The hypothesis of axial symmetry seems to be reasonable because of the lateral heating, provided the aspect ratio be kept close to unity. The flow is governed by the macroscopic conservation equations written for an incompressible, Newtonian, zero-bulk-viscosity fluid. Besides, we apply the Boussinesq approximation, that is to say, density variations are taken into account only in the buoyancy term of the Navier–Stokes equation under the form $\rho = \rho_0(1-\beta(T'-T'_0))$. In the energy equation, we neglect compression work and viscous dissipation. Considering the fluids to be opaque or transparent in the infrared, radiative flux divergence doesn't occur. Furthermore, except for the density in the Navier–Stokes equation, all physical properties are assumed to be constant. We obtain the following set of so-called Boussinesq equations written in their non-conservative form:

equation of continuity:

$$\nabla . V' = 0 \qquad (1)$$

equation of momentum:

$$\rho_0 \frac{\mathrm{d}V'}{\mathrm{d}t'} = -\rho_0\beta(T'-T'_0)\mathbf{g} - \nabla p^* + \mu\nabla^2 V' \qquad (2)$$

equation of energy:

$$\frac{\mathrm{d}T'}{\mathrm{d}t'} = a\nabla^2 T' \qquad (3)$$

To write the equations in axisymmetric coordinates we use the differential operators:

NOMENCLATURE

a	thermal diffusivity [$m^2 s^{-1}$]
Al	aspect ratio, H/D
D	dimensional diameter [m]
g	gravity [$m s^{-2}$]
Gr	Grashof number, $g\beta\Delta T_0 H^3/\nu^2$
H	dimensional height of the cylinder [m]
$\bar{h}$	average heat transfer coefficient [$W m^{-2} K^{-1}$]
$Nu_{b,t}$	Nusselt numbers (Rayleigh configuration)
$Nu_{c,l}$	Nusselt numbers (lateral heating configuration)
Pr	Prandtl number, ν/a
p^*	hydrostatic pressure, $p+\rho_0 gz$ [Pa]
R	Rayleigh number (Rayleigh configuration)
Ra	Rayleigh number (lateral heating configuration), $g\beta\Delta T_0 H^3/a\nu$
r	dimensionless radial coordinate
T	dimensionless temperature
T_s	dimensionless average temperature of sidewall
T_m	dimensionless average temperature of fluid
t	dimensionless time
V	dimensionless velocity
u	dimensionless radial velocity
v	dimensionless axial velocity
z	dimensionless axial coordinate.

Greek symbols

β	thermal expansion coefficient [K^{-1}]
Δr	dimensionless radial grid size
Δz	dimensionless axial grid size
ε	relative error in convergence criteria
λ	thermal conductivity [$W m^{-1} K^{-1}$]
μ	dynamic viscosity [$N s m^{-2}$]
ν	kinematic viscosity [$m^2 s^{-1}$]
ξ	dimensionless temperature or dimensionless modified vorticity
ρ	density [$kg m^{-3}$]
Φ	lateral flux density [$W m^{-2}$]
ψ	dimensionless stream function
ω	dimensionless vorticity
Ω	dimensionless modified vorticity, $r\omega$.

Subscripts

b	bottom of the cylinder
c	roof of the cylinder
ce	centre of the computational domain
l	sidewall of the cylinder
max	maximum value
min	minimum value
0	reference value
t	top surface of the cylinder.

Superscript

$'$	dimensional variable (used when a dimensionless variable of the same name occurs)
k, n	iteration indexes.

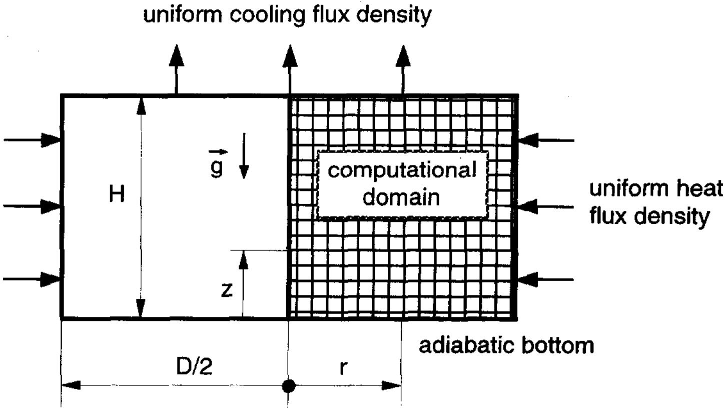

Fig. 1. Vertical cross-section of the studied geometry.

$$\nabla = \frac{\partial}{\partial r'} + \frac{\partial}{\partial z'} \tag{4}$$

$$\nabla . = \frac{1}{r'}\frac{\partial}{\partial r'}r' + \frac{\partial}{\partial z'} \tag{5}$$

$$\nabla^2 = \frac{\partial^2}{\partial r'^2} + \frac{1}{r'}\frac{\partial}{\partial r'} + \frac{\partial^2}{\partial z'^2} \tag{6}$$

$$[\nabla^2 V']_{r'} = \nabla^2 u' - \frac{u'}{r'^2} \tag{7}$$

$$[\nabla^2 V']_{z'} = \nabla^2 V'. \tag{8}$$

The equations become in the (r', z') coordinates:

$$\frac{\partial u'}{\partial r'} + \frac{\partial v'}{\partial z'} + \frac{u'}{r'} = 0 \tag{9}$$

$$\frac{\partial u'}{\partial t'} + u'\frac{\partial u'}{\partial r'} + v'\frac{\partial u'}{\partial z'} = -\frac{1}{\rho_0}\frac{\partial p^*}{\partial r'} + v\left(\frac{\partial^2 u'}{\partial r'^2} + \frac{1}{r'}\frac{\partial u'}{\partial r'} + \frac{\partial^2 u'}{\partial z'^2} - \frac{u'}{r'^2}\right) \tag{10}$$

$$\frac{\partial v'}{\partial t'} + u'\frac{\partial v'}{\partial r'} + v'\frac{\partial v'}{\partial z'} = \beta(T' - T'_0)g - \frac{1}{\rho_0}\frac{\partial p^*}{\partial z'} + v\left(\frac{\partial^2 v'}{\partial r'^2} + \frac{1}{r'}\frac{\partial v'}{\partial r'} + \frac{\partial^2 v'}{\partial z'^2}\right) \tag{11}$$

$$\frac{\partial T'}{\partial t'} + u'\frac{\partial T'}{\partial r'} + v'\frac{\partial T'}{\partial z'} = a\left(\frac{\partial^2 T'}{\partial r'^2} + \frac{1}{r'}\frac{\partial T'}{\partial r'} + \frac{\partial^2 T'}{\partial z'^2}\right). \tag{12}$$

We write equations (9)–(12) in the stream function–vorticity formalism by defining:

$$u' = \frac{1}{r'}\frac{\partial \psi'}{\partial z'} \tag{13}$$

$$v' = -\frac{1}{r'}\frac{\partial \psi'}{\partial r'} \tag{14}$$

$$\omega' = \frac{\partial u'}{\partial z'} - \frac{\partial v'}{\partial r'}. \tag{15}$$

To simplify the equations, it is useful to set $\Omega' = r'\omega'$. We choose as the length scale the height H of the cylinder. We use the initial temperature of the system T'_0 and $\Delta T'_0 = \Phi H/\lambda$ as the reference temperature and reference temperature difference, respectively. The velocity scale is the velocity of a fluid particle which would be accelerated over H without viscous force, that is to say $V'_0 = \sqrt{gH\beta\Delta T'_0}$. The time scale is obviously defined as H/V'_0. With these reference values, we define the following dimensionless variables: $T = (T' - T'_0)/\Delta T'_0$, $\psi = \psi'/(V'_0 H^2)$ and $\Omega = \Omega'/V'_0$. In their dimensionless form, the equations become:

$$-\Omega - \frac{1}{r}\frac{\partial \psi}{\partial r} + \frac{\partial^2 \psi}{\partial r^2} + \frac{\partial^2 \psi}{\partial z^2} = 0 \tag{16}$$

$$\frac{\partial \Omega}{\partial t} = -r\frac{\partial T}{\partial r} + \frac{2}{r^2}\frac{\partial \psi}{\partial z}\Omega - \frac{1}{r}\left(\frac{\partial \psi}{\partial z} + \frac{1}{\sqrt{Gr}}\right)\frac{\partial \Omega}{\partial r} + \frac{1}{r}\frac{\partial \psi}{\partial r}\frac{\partial \Omega}{\partial z} + \frac{1}{\sqrt{Gr}}\left(\frac{\partial^2 \Omega}{\partial r^2} + \frac{\partial^2 \Omega}{\partial z^2}\right) \tag{17}$$

$$\frac{\partial T}{\partial t} = \frac{1}{r}\left(\frac{1}{Pr\sqrt{Gr}} - \frac{\partial \psi}{\partial z}\right)\frac{\partial T}{\partial r} + \frac{1}{r}\frac{\partial \psi}{\partial r}\frac{\partial T}{\partial z} + \frac{1}{Pr\sqrt{Gr}}\left(\frac{\partial^2 T}{\partial r^2} + \frac{\partial^2 T}{\partial z^2}\right). \tag{18}$$

The initial and boundary conditions are expressed as:

at $t = 0$:

$$\psi(r, z, 0) = 0 \tag{19}$$

$$\Omega(r, z, 0) = 0 \tag{20}$$

$$T(r, z, 0) = 0 \tag{21}$$

on $r = 0$:

$$\psi = \frac{\partial \psi}{\partial z} = 0 \tag{22}$$

$$\Omega = 0 \tag{23}$$

$$\frac{\partial T}{\partial r} = 0 \tag{24}$$

on $r = 1/(2Al)$:

$$\psi = \frac{\partial \psi}{\partial z} = \frac{\partial \psi}{\partial r} = 0 \tag{25}$$

$$\Omega = \frac{\partial^2 \psi}{\partial r^2} \tag{26}$$

$$\frac{\partial T}{\partial r} = \frac{H\Phi}{\lambda \Delta T'_0} = 1 \tag{27}$$

on $z = 0$:

$$\psi = \frac{\partial \psi}{\partial z} = \frac{\partial \psi}{\partial r} = 0 \tag{28}$$

$$\Omega = \frac{\partial^2 \psi}{\partial z^2} \tag{29}$$

$$\frac{\partial T}{\partial z} = 0 \tag{30}$$

on $z = 1$:

$$\psi = \frac{\partial \psi}{\partial z} = \frac{\partial \psi}{\partial r} = 0 \tag{31}$$

$$\Omega = \frac{\partial^2 \psi}{\partial z^2} \tag{32}$$

$$\frac{\partial T}{\partial z} = -\frac{4HAl\Phi}{\lambda \Delta T'_0} = -4Al. \tag{33}$$

The last condition describes the heat loss of the laterally entering flux through the top of the domain in order to obtain a steady-state solution.

3. NUMERICAL METHOD AND ALGORITHM

The non-conservative form of the equations is discretized using a finite-difference method on a uniform grid. At first, the energy and vorticity equations are solved by the A.D.I. method [6], a purely implicit scheme in one direction over a half time step. The elliptic equation of the stream function is then solved by the over-relaxation Gauss–Seidel method. To allow a transient simulation, this last equation is solved at each time step, i.e. internal iterations are necessary to ensure the convergence. This iterative technique stops when the following convergence criterion is respected:

$$\frac{\max|\psi^{k+1}-\psi^{k}|}{\max|\psi^{k}|} < 10^{-4}. \tag{34}$$

The over-relaxation coefficient is chosen as 1.725. While the central difference scheme is systematically used for the diffusion terms, the hybrid central/upwind difference scheme is used for the convective terms according to the local value of the grid Peclet number. The resulting tridiagonal linear systems are solved by the Thomas algorithm [7] which is not only fast but also convenient to treat the singularity at $r = 0$ often critical in cylindrical coordinates because of the $1/r$ terms in the basic equations. In this algorithm, only the interior points are calculated by means of the basic equations obviously taking the boundary values into account. These boundary points are not calculated by means of the conservation equations but are derived from Taylor series expansions of adjacent points. Besides, the axial velocity showed at $r = 0$ on the figures is calculated by a three points Taylor serie expansion using the fact that $\partial v/\partial r = 0$ at $r = 0$. This procedure is only first-order accurate but this axial velocity is only used in the data processing. Before reaching the next time step, internal iterations are made to find the velocity of the convective terms: this procedure ensures an efficient coupling of the equations by these strongly non-linear terms, and second-order temporal precision in the A.D.I. method [8]. To keep a reasonable CPU time, one or two internal iterations are generally carried out. Lastly, average temperature of fluid and average temperature of sidewall are calculated by the Riemann integration method with

$$T_{\mathrm{m}} = 8Al^{2}\int_{0}^{1}\int_{0}^{1/(2Al)} Tr\,\mathrm{d}r\,\mathrm{d}z, \quad T_{\mathrm{s}} = \int_{0}^{1} T_{\mathrm{l}}\,\mathrm{d}z. \tag{35}$$

In this paper, all the simulations result from transient calculations, in the sense that the Poisson equation is always correctly solved, so the steady-state solutions constitute the final states of the transient calculations. Numerically, we call 'steady-state' the solution reached when the code has converged, satisfying a criterion of the kind:

$$\frac{\max|\xi^{n+1}-\xi^{n}|}{\max|\xi^{n}|} < \varepsilon \tag{36}$$

where ξ is T and Ω. ε is taken to be compatible with the time step so that the code marches far enough in time to describe the transient regime before reaching a steady-state. This is done by monitoring the transient evolution of several values, such as the stream function at the centre of the computational domain. In most cases, for a typical time step of 10^{-2}, ε is chosen to be 10^{-7}. All numerical simulations result from vectorized calculations performed on Cray C94 and C98. The time of a typical calculation, for an 81 × 81 uniform grid, is on order of 15 min CPU.

4. NUMERICAL TESTS

4.1. *Rayleigh configuration*

We have tested our code by investigating the flow which occurs in a fluid layer in the Rayleigh configuration, i.e. heated from below and cooled from above with isothermal top and bottom walls and with an insulated lateral wall. No-slip conditions are assumed at all walls.

Figure 2 shows the cross-section of the stationary solution of the flow in an air-filled cylinder for $Al = 1/2$, $R = 5000$ and $Pr = 0.7$. An 81 × 81 uniform grid was fine enough to obtain the average Nusselt number Nu_{b} at the bottom nearly identical to the average Nusselt number Nu_{t} at the top (conservation of the energy). Nu_{b} and Nu_{t} are defined by:

$$Nu_{\mathrm{b,t}} = 8Al^{2}\int_{0}^{1/(2Al)} -\left.\frac{\partial T}{\partial z}\right|_{\mathrm{b,t}} r\,\mathrm{d}r. \tag{37}$$

The relative difference between Nu_{b} and Nu_{t} is less than 1%. These simulations confirm two interesting features of the flow already pointed out by Liang *et al.* [4]. It is also particularly interesting to compare our results with the 3D calculations of an axisymmetric flow performed by Schneider *et al.* [9]. The convective flow depends on the initial temperature field. In our example, setting initial temperatures to zero everywhere induces an upflow at the centre of the cylinder. On the contrary, if buoyancy is increased by initial conditions, for instance with an initial hot penultimate column of the computational domain, a downflow is induced at the centre. It can also be seen that the centre of the toroidal roll is slightly shifted upwards in the case of upflow and downwards in the case of downflow. This asymmetry has been encountered both numerically and experimentally by Liang *et al.* [4].

4.2. *Lateral heating and upper cooling at uniform flux density*

To determine the influence of the mesh, we respectively tested 21 × 21, 41 × 41, and 81 × 81 uniform

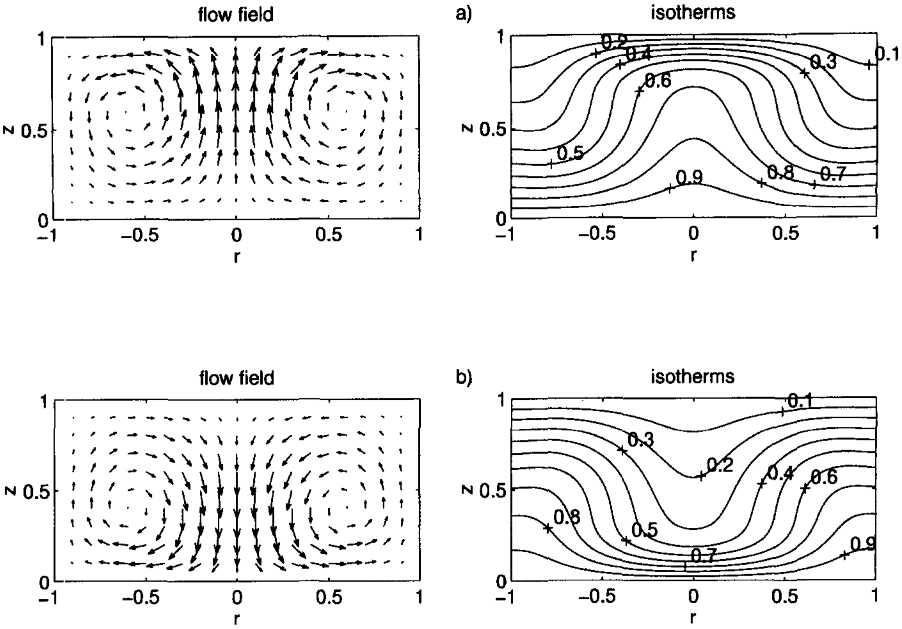

Fig. 2. Stationary flow in the Rayleigh configuration; $Al = 1/2$; $R = 5000$; $Pr = 0.7$; (a) upflow at the centre, $V_{max} = 0.353$; (b) downflow at the centre, $V_{max} = 0.353$.

Table 1. Mesh influence

Mesh	21 × 21	41 × 41	81 × 81	221 × 221
T_{ce}	0.1282×10^{-1}	0.1880×10^{-1}	0.2001×10^{-1}	0.1993×10^{-1}
ψ_{ce}	0.2176×10^{-1}	0.1991×10^{-1}	0.2008×10^{-1}	0.2013×10^{-1}
V_{max}	0.4706	0.4548	0.4550	0.4552
Nu_c	28.96	25.36	24.29	23.99
Nu_l	14.02	14.59	14.42	14.37

grids by comparing results with a reference calculation performed on a 221 × 221 regular mesh. The parameters of these simulations are $Gr = 1.4 \times 10^5$, i.e. $Ra = 10^5$, $Pr = 0.7$ and $Al = 1/2$. We first ensured energy conservation, which is not guaranteed by a non-conservative discretization. Initializing all the temperatures to zero, the dimensionless average temperature of the stationary solution is on order of 10^{-4}. By monitoring several variables, Table 1 indicates that a 41 × 41 mesh can be adequate. However, Figs. 3 and 4 show that the 81 × 81 grid ensures a better resolution of the near-wall flows. As the calculation times remain reasonable, the 81 × 81 uniform grid is used or, more exactly, as we vary the aspect ratio, in most cases we keep a constant resolution of $\Delta r = \Delta z = 1.25 \times 10^{-2}$.

5. RESULTS AND DISCUSSION

For the purpose of this parametric study, the dimensionless numbers varied over the following ranges:

$$10^2 \leqslant Ra \leqslant 10^6 \tag{38}$$

$$0.7 \leqslant Pr \leqslant 92.5 \tag{39}$$

$$1/5 \leqslant Al \leqslant 2. \tag{40}$$

Although the code is not theoretically the best adapted to detect the eventual appearance of a physically oscillating final state because of the damping effect of the hybrid scheme, it is interesting to note that the maximum Grashof number at which a steady-state is reached decreases as the cylinder becomes flatter. This seems logical since an increasingly flatter cylinder 'forgets' the stabilizing effect of the sidewall as it nears the Rayleigh configuration. Because of the upper cooling, we must keep in mind that our problem is a combination of Rayleigh and lateral heating configurations. In the former, it is well known that stable axisymmetric solutions are limited to small Rayleigh numbers [1, 9]. So it was felt that the assumption of two-dimensional flow could be more and more hazardous as the aspect ratio becomes smaller and consequently could make some results of the parametric study unrealistic for high Rayleigh number/small aspect ratio configuration where a linear stability analysis or 3D calculations should be necessary to assess the validity of the axial symmetry assumption.

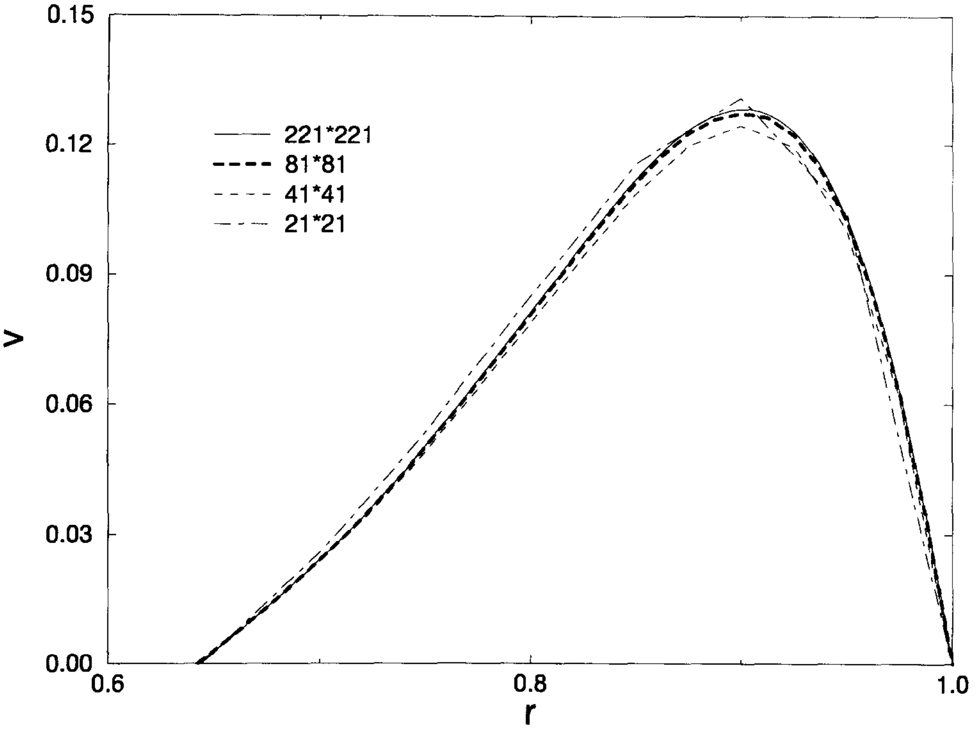

Fig. 3. Vertical velocity profile near sidewall at $z = 0.5$; $Ra = 10^5$; $Pr = 0.7$; $Al = 1/2$.

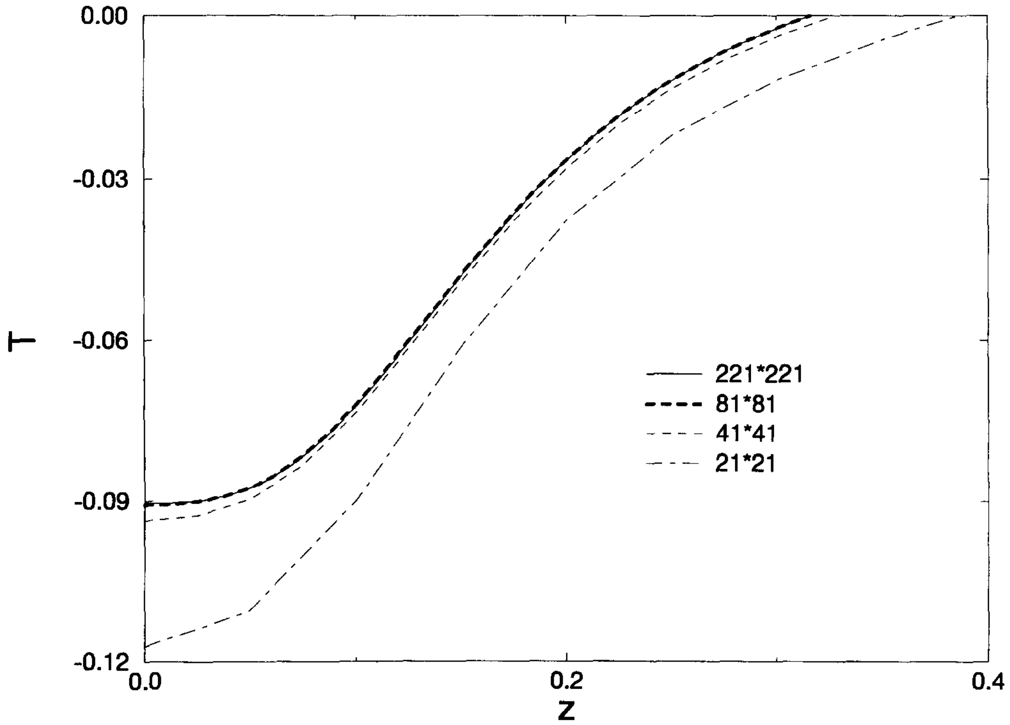

Fig. 4. Temperature vertical profile near bottom at $r = 0.5$; $Ra = 10^5$; $Pr = 0.7$; $Al = 1/2$.

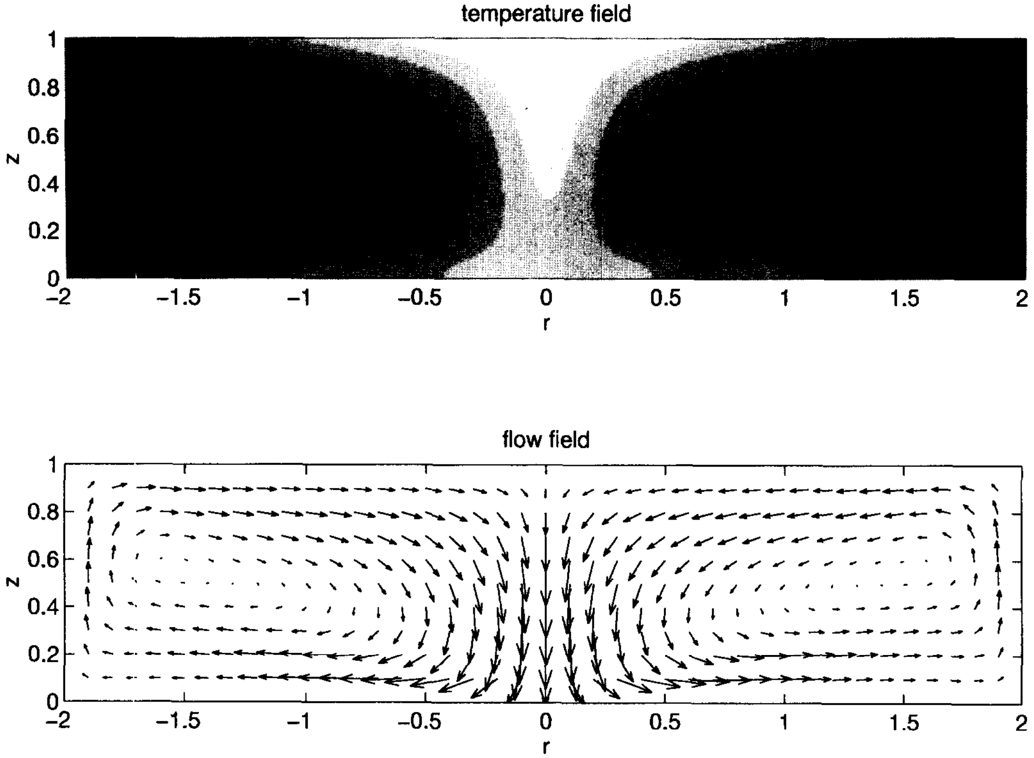

Fig. 5. Stationary flow under lateral heating; $Al = 1/4$; $Ra = 10^5$; $Pr = 0.7$; $T_{\max}$ (black) $= 0.23$; $T_{\min}$ (white) $= -0.39$; $V_{\max} = 0.352$.

Nevertheless, we have made small aspect ratio calculations for two reasons:

- we believe that the influence of the lateral heating is still important for small aspect ratio, provided we restrict to steady-state flows;
- real cylindrical tanks are often partially filled and result in small aspect ratio fluid domain ($Al \leqslant 1$).

In this paper, the maximum calculated Grashof number—the parameter effectively present in the equations—is $Gr = 1.4 \times 10^6$, which corresponds to the cases $Ra = 10^6$, $Pr = 0.7$ and $Al \geqslant 1/2$. The Prandtl numbers range is over three orders of magnitude. $Pr = 0.7$ corresponds to air and, more generally, most gases at 300 K. $Pr = 7$ corresponds to water at 293 K and $Pr = 92.5$ corresponds to ethylene glycol at 313 K.

We first present stationary solutions and their sensibility to the control parameters. We then consider the transient behaviour of the fluid flow.

5.1. *Stationary solutions*

Flow structure and temperature field. Perhaps the most important feature to mention is that, in all cases studied, the flow presents a single toroidal roll (Figs. 5–8). This structure is conserved even at a relatively flat aspect ratio ($Al \leqslant 1/4$). The plotted velocity vectors show clearly that the flow is much faster in the centre, obviously to ensure mass conservation in a horizontal cross-section. Figure 9 shows the influence of the Rayleigh number for an air-filled box with $Al = 1/2$. At low Ra, near a conductive regime, the isotherms are slightly deformed by the movement, with the highest temperature in the lower corner of the cylinder. As Ra increases, the isotherms become much more deformed with a clear homogenization of the hot area along the sidewall due to the upward buoyancy-induced flow. In Figs. 5–8, the temperature fields show that the 'cold zone' expands on the sidewall as the aspect ratio increases. It must be noted that the minimum temperature, obviously located at the centre of the cold ceiling, decreases as the aspect ratio increases, while the maximum temperature remains almost constant between $Al = 1/5$ and $Al = 1$. Furthermore, the maximum temperature at the sidewall is located in the range $0.7 \leqslant z \leqslant 1$. We note that this maximum approaches $z = 1$ as Al increases from 0.25 to 1, both for $Pr = 0.7$ and $Pr = 7$. In the case of gases ($Pr = 0.7$) and $Al = 2$, the maximum sidewall temperature is located at the bottom ($z = 0$), which is coherent with the fact that the 'cold zone' expands as the aspect ratio increases. It can also be observed that the Prandtl number affects the flow structure. As illustrated in Fig. 10, the centre of the toroidal roll is

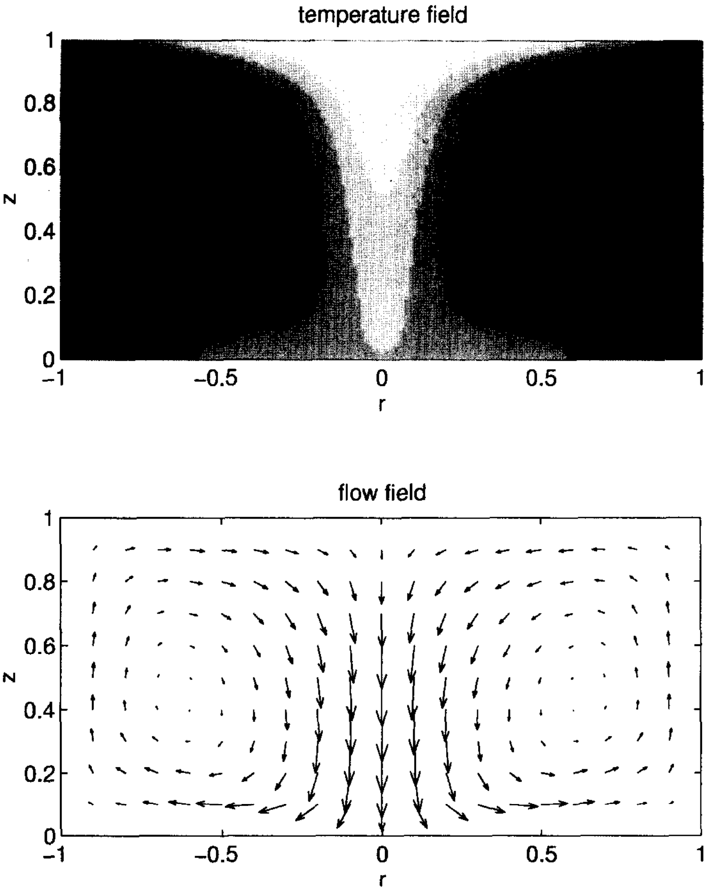

Fig. 6. Stationary flow under lateral heating; $Al = 1/2$; $Ra = 10^5$; $Pr = 0.7$; $T_{\max}$ (black) = 0.21; $T_{\min}$ (white) = −0.52; $V_{\max} = 0.455$.

shifted below the $z = 0.5$ plane as Pr decreases. The maximum velocity (plotted in Figs. 11 and 12) gives an idea of the intensity of the flow. Increasing the Ra number enhances the maximum velocity. For $Al = 1/2$ and a constant Ra, there is an increase of the maximum velocity with decreasing Prandtl number. Figure 12 shows the influence of the aspect ratio on the maximum velocity, for $Pr = 0.7$. For $Ra \leqslant 2.5 \times 10^4$, the maximum velocity is attained for $Al = 1/2$. When $Ra > 2.5 \times 10^4$, the maximum is attained for $Al = 1$.

Heat transfer. The average Nusselt numbers are defined by the following equations:

At the sidewall: $Nu_l = \bar{h}D/\lambda$, where $\bar{h} = \Phi/(T'_s - T'_m)$

$$\Rightarrow Nu_l = 1/(Al|T_s - T_m|). \qquad (41)$$

At the top of the domain: $Nu_c = \bar{h}D/\lambda$, where $\bar{h} = 4Al\Phi/(T'_m - T'_s)$

$$\Rightarrow Nu_c = 4/(|T_m - T_s|). \qquad (42)$$

Figure 13 shows that the convection heat transfer both on the side and the top of the domain does not explicitly depend on the Prandtl number (we except the implicit dependence since the Rayleigh number definition includes the Prandtl number) that is to say $Nu_{c,l}$ depends on the product $Gr^x Pr^y$ where the powers x and y are identical. Thus in this case the Rayleigh number is more convenient to describe the convection heat transfer. For the case plotted, $Al = 1/2$ but the result is confirmed for $Al = 1/4$ and $Al = 1$. In Fig. 14, for a Prandtl number of 0.7 and varying Al in the range $1/5 \leqslant Al \leqslant 2$, we see that the convective heat transfer at the top of the domain is enhanced by increasing Ra and decreasing Al for a constant Ra number, but two kinds dependence of evolution clearly exist: for $Al > 1/3$, the Nusselt number increases with the same concavity. In this case, the following numerical correlation has been found (Fig. 15):

$$Nu_c = 0.55Al^{-1.25}Ra^{0.25} \qquad (43)$$

with $10^2 \leqslant Ra \leqslant 10^6$ and $1/2 \leqslant Al \leqslant 2$.

For the case where $Al < 1/3$, the graphs present an inflection point, that is to say the increasing heat transfer is enhanced for $10^3 < Ra < 10^4$. The lateral convective heat transfer (Fig. 16), as at the top of the

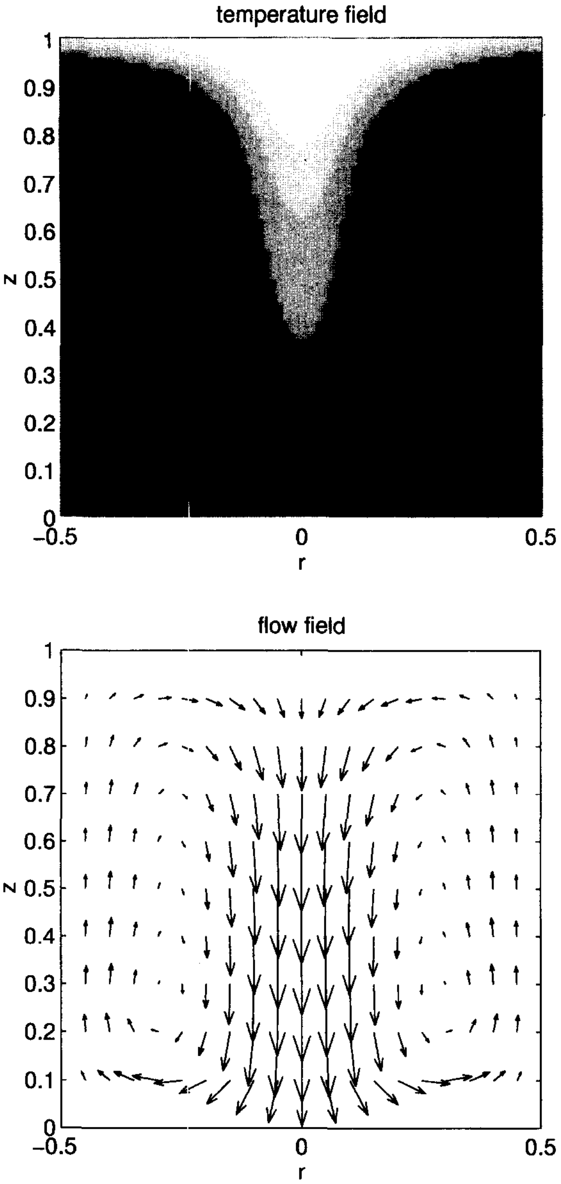

Fig. 7. Stationary flow under lateral heating; $Al = 1$; $Ra = 10^5$; $Pr = 0.7$; T_{max} (black) $= 0.22$; T_{min} (white) $= -0.74$; $V_{max} = 0.482$.

cylinder, is enhanced with increasing Ra and decreasing Al for a constant Ra number, except for $Al = 1$ and $Al = 2$ where the heat transfer is little influenced by Ra. The following correlations have been found (Figs. 17 and 18):

$$Nu_l = 0.86 Al^{-0.75} Ra^{0.2} \quad (44)$$

with $10^4 \leqslant Ra \leqslant 10^6$ and $1/2 \leqslant Al \leqslant 1$

$$Nu_l = 0.54 Al^{-0.74} Ra^{0.24} \quad (45)$$

with $10^3 \leqslant Ra \leqslant 10^5$ and $1/5 \leqslant Al \leqslant 1/3$.

Finally, Figs. 14–16 show that the convective heat transfer is more important at the top surface for $1/5 \leqslant Al \leqslant 1/2$, even when the lateral surface becomes larger than the top surface, that is when $Al \geqslant 1/4$.

5.2. *Transient calculations*

For $Pr = 0.7$ and $Pr = 7$, the study of the transient phase before reaching a steady-state reveals an interesting behaviour. A two-roll solution has indeed been found: this flow structure is time-limited and occurs when the cylinder is flat enough, that is when $Al \leqslant 1/3$ at $Ra = 10^5$, both for $Pr = 0.7$ and $Pr = 7$. Figure 19 shows a transient sequence for $Ra = 10^5$, $Pr = 7$ and $Al = 1/3$. Initially, a single roll develops near the sidewall of the cylinder. Then the roll progressively grows with a concomitant inward shift to the centre of the cell. At $t = 21$, a second roll is induced near the top surface: an upflow is consequently induced at the centre of the cylinder. The first counterclockwise roll continues to grow until it becomes predominant. Finally, the flow becomes unicellular again at $t = 42$ and this single roll structure remains until the steady-state has been reached. The occurrence of this two-roll transient flow seems to be a general feature encountered by several authors in different configurations and scales, studying petroleum flow in a cylindrical tank [10], solidification in a rectangular enclosure [11] or cooling of a square cavity [12]. In our case, this structure may be explained in the following way: initially, the near sidewall roll is not vigorous enough to extend over the entire cylinder. The fluid rises along the sidewall and turns at the top sidewall corner and moving inward under the top surface. The top surface cools this inward flow which becomes denser, and the fluid moves away from the sidewall effect, that is from the origin of the buoyancy forces. The influence of the viscous forces then becomes important and consequently, the inward flow decelerates and turns downward. There is then probably a drawing effect which induces a clockwise roll which subsits until the counterclockwise roll becomes energetic enough to overcome the second cell. Furthermore, as suggested by Cotter and Charles [10], vorticity can be generated by a radial temperature gradient, as can be seen from equation (17). In the near sidewall roll the upward flow carries hot fluid inducing a positive radial temperature gradient which in turn induces negative vorticity. The two-roll flow could result from a combination of the drawing effect and temperature gradient generated vorticity.

6. CONCLUSION

In this work, numerical simulations have been performed in order to study the buoyancy-induced flow in a laterally heated vertical cylinder. By varying the dimensionless numbers which characterize the problem and by examining the flow structure, the following points can be made. All the stationary solutions present a single roll pattern. The convective heat transfer does not explicitly depend on the Prandtl number. On the contrary, the convective heat transfer is enhanced

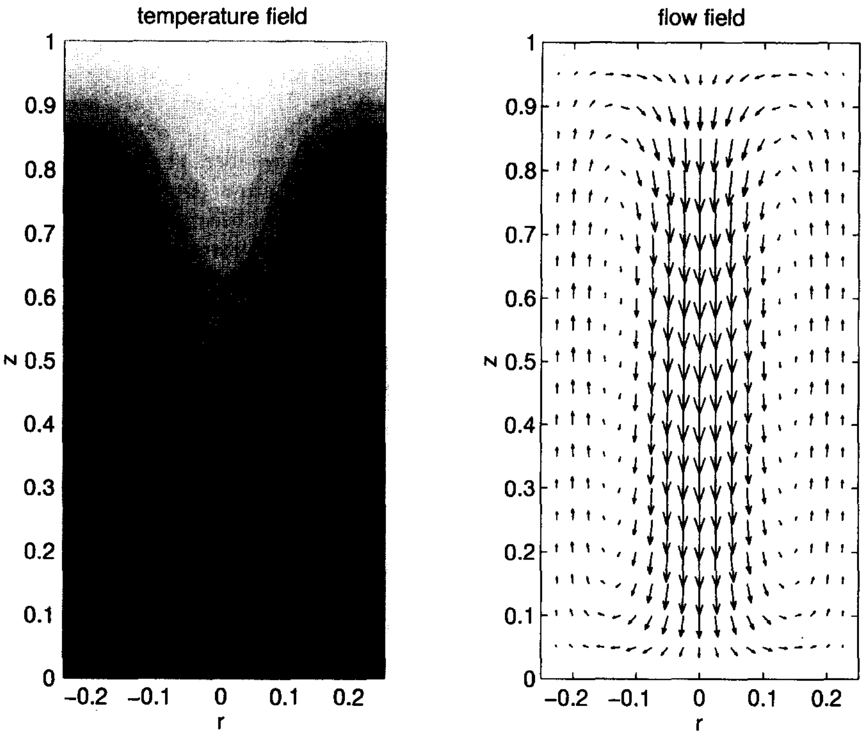

Fig. 8. Stationary flow under lateral heating; $Al = 2$; $Ra = 10^5$; $Pr = 0.7$; $T_{\max}$ (black) $= 0.36$; $T_{\min}$ (white) $= -1.42$; $V_{\max} = 0.358$.

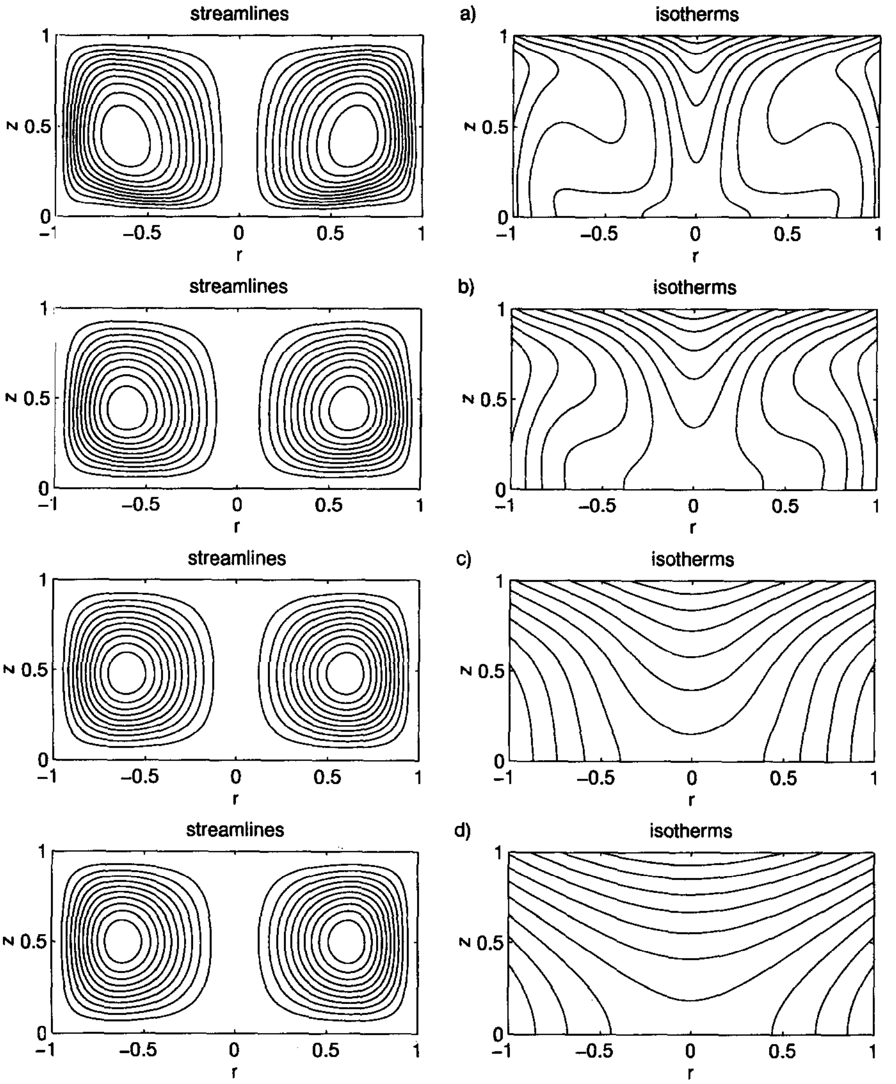

Fig. 9. Streamlines and isotherms for $Al = 1/2$ and $Pr = 0.7$; (a) $Ra = 10^5$, $T_{\max} = 0.21$, $T_{\min} = -0.52$, $\Delta T = 0.066$, $\psi_{\max} = 0.0224$; (b) $Ra = 10^4$, $T_{\max} = 0.30$, $T_{\min} = -0.69$, $\Delta T = 0.09$, $\psi_{\max} = 0.0307$; (c) $Ra = 10^3$, $T_{\max} = 0.50$, $T_{\min} = -0.93$, $\Delta T = 0.13$, $\psi_{\max} = 0.02$; (d) $Ra = 10^2$, $T_{\max} = 0.58$, $T_{\min} = -0.92$, $\Delta T = 0.137$, $\psi_{\max} = 0.0044$.

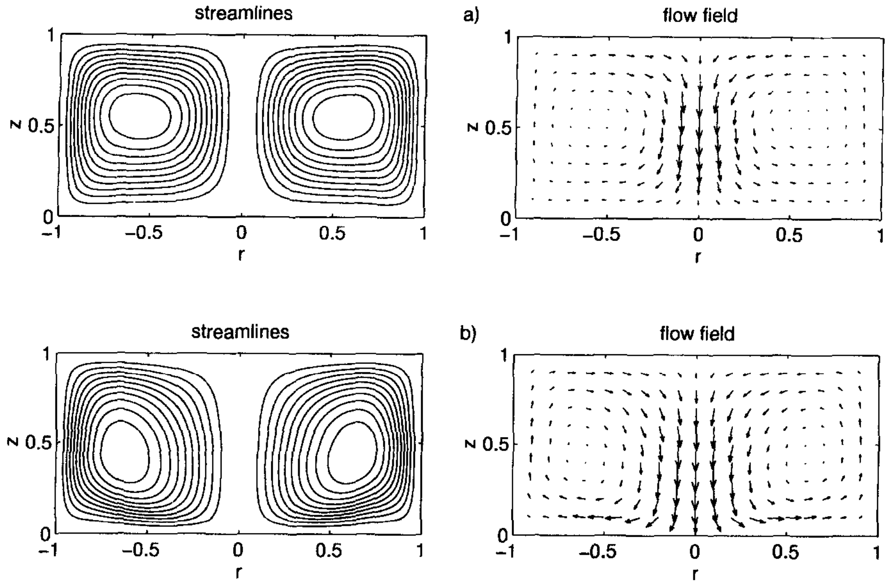

Fig. 10. Streamlines and flow field for $Al = 1/2$ and $Ra = 10^5$; (a) $Pr = 92.5$, $V_{max} = 0.07$, $\psi_{max} = 0.0022$; (b) $Pr = 0.7$, $V_{max} = 0.455$, $\psi_{max} = 0.0224$ (flow fields have different velocity scales).

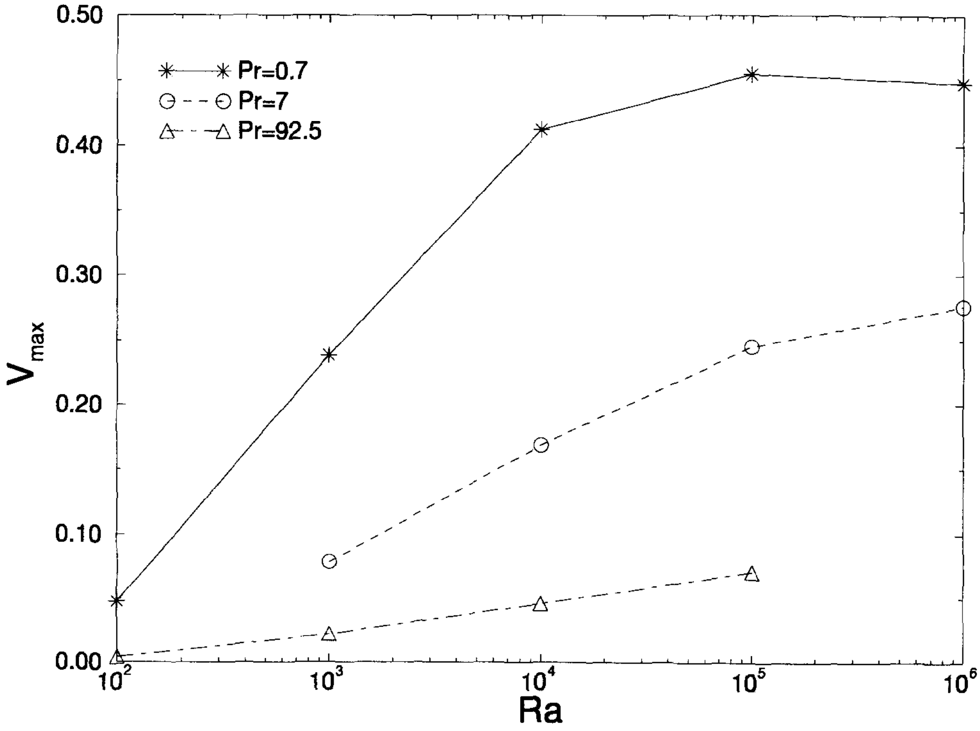

Fig. 11. Maximum velocity vs Rayleigh number for various Prandtl numbers ($Al = 1/2$).

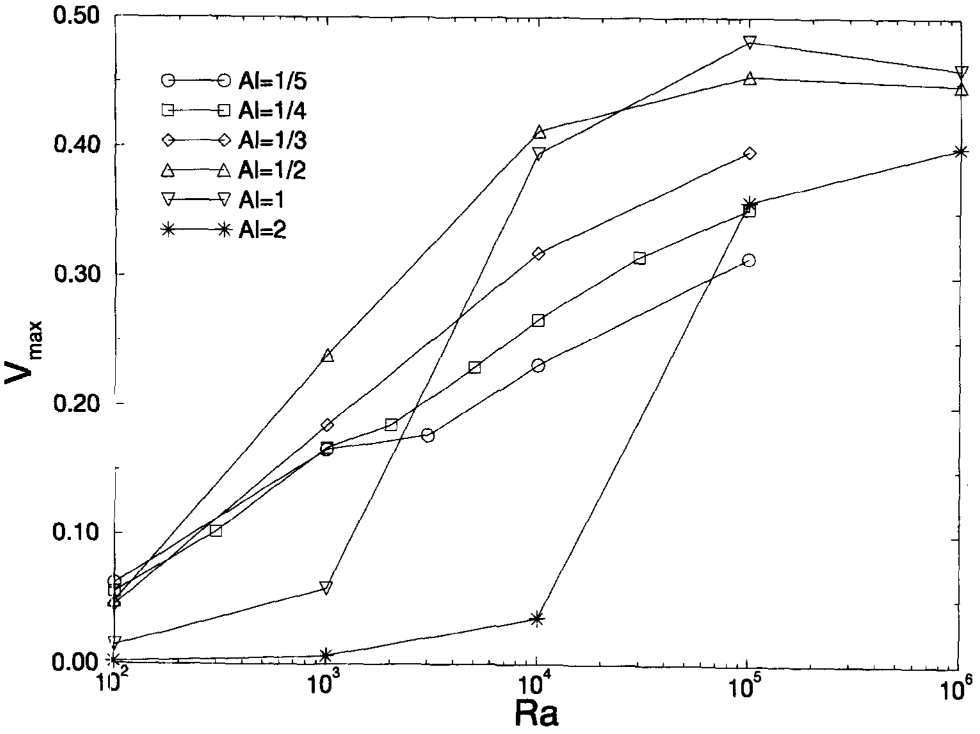

Fig. 12. Maximum velocity vs Rayleigh number for various aspect ratios ($Pr = 0.7$).

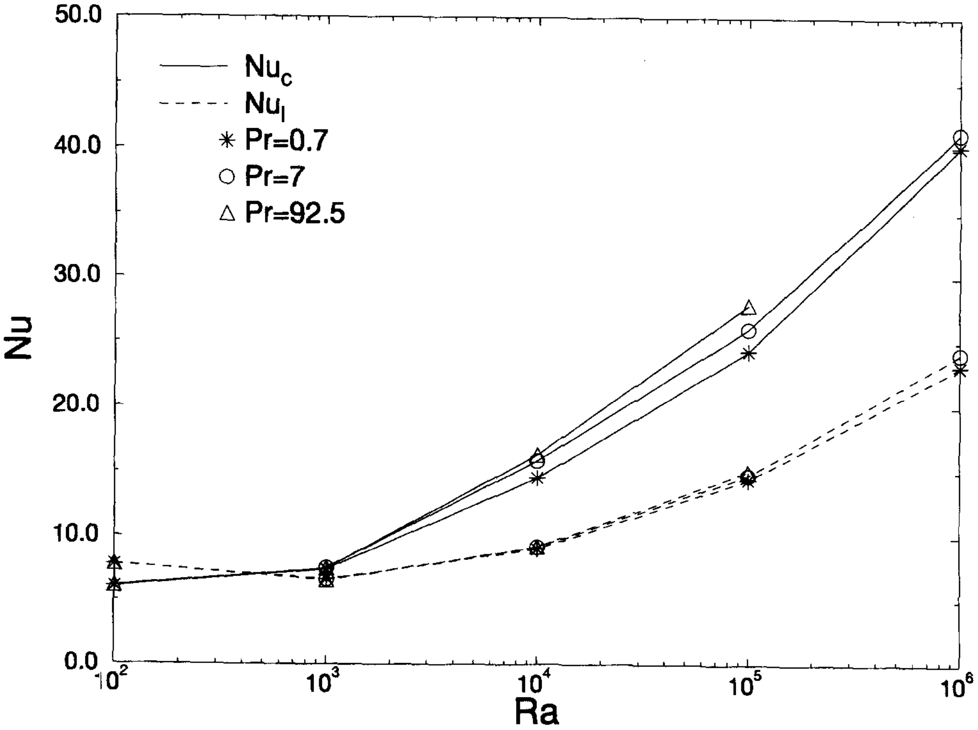

Fig. 13. Top and lateral average Nusselt number vs Rayleigh number for various Prandtl numbers ($Al = 1/2$).

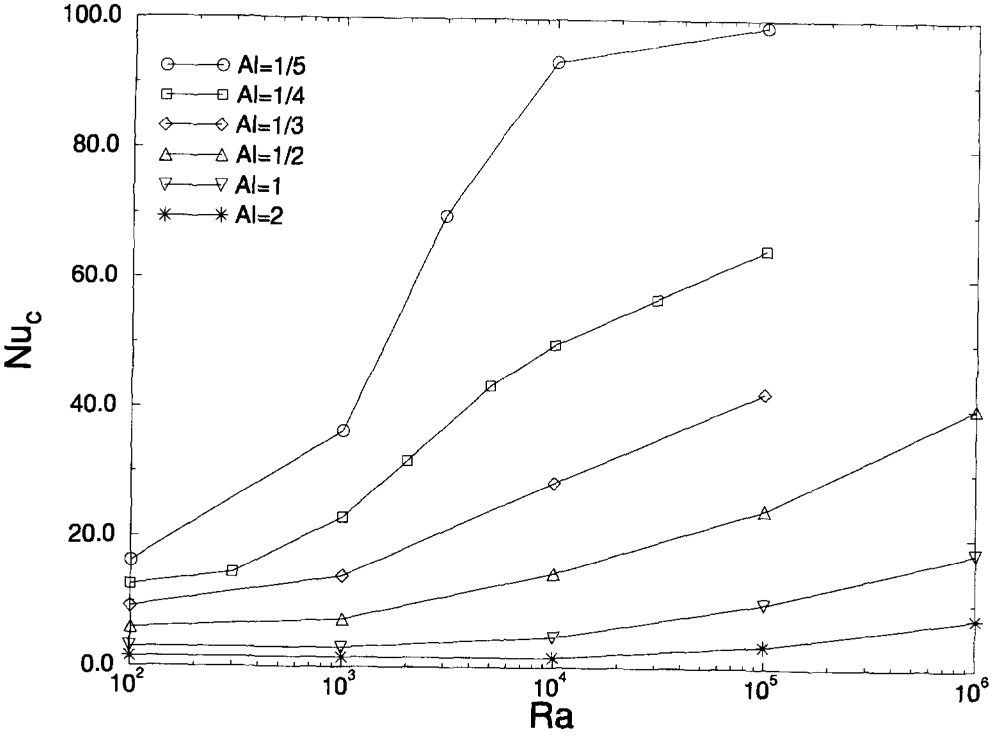

Fig. 14. Top Nusselt number vs Rayleigh number for various aspect ratios ($Pr = 0.7$).

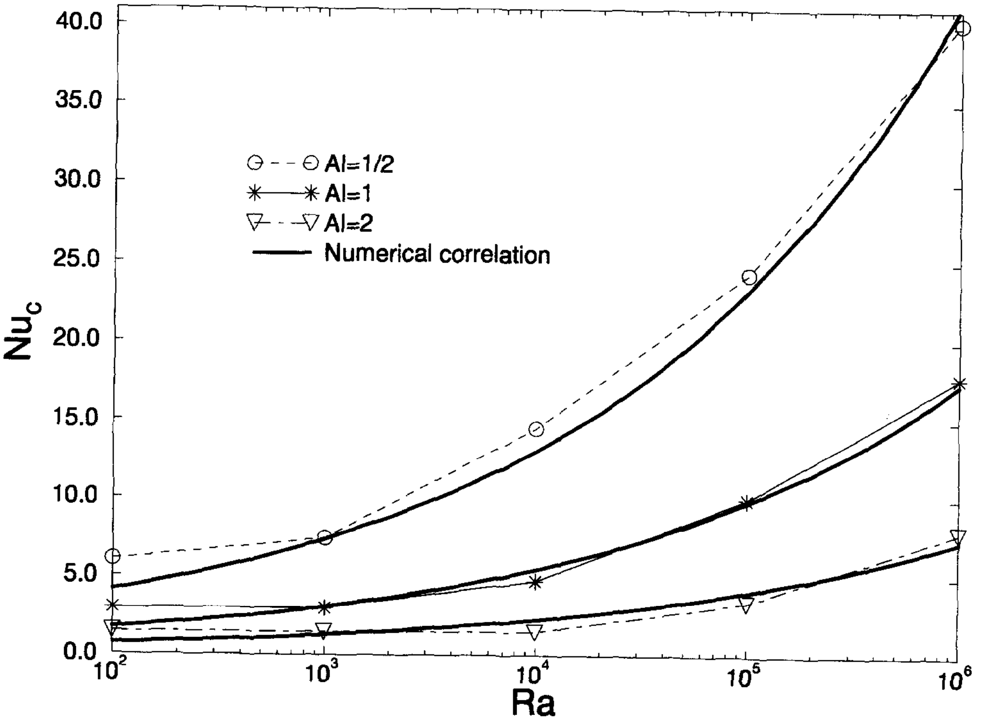

Fig. 15. Top Nusselt number vs Rayleigh number and numerical correlation $Nu_c = 0.55Al^{-1.25}Ra^{0.25}$.

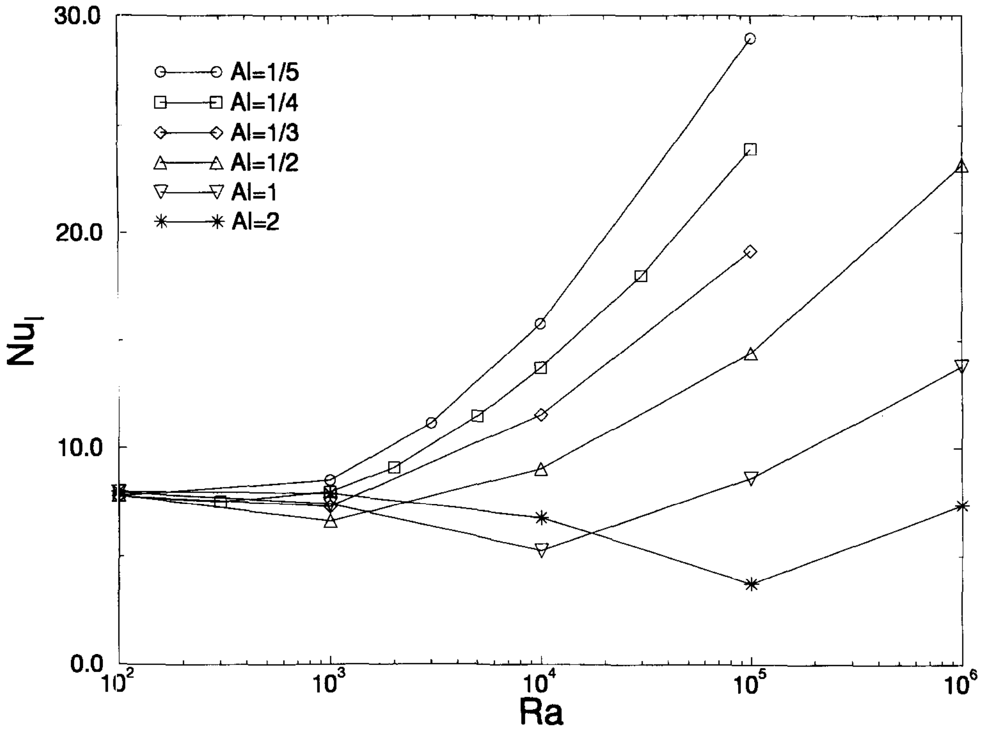

Fig. 16. Lateral Nusselt number vs Rayleigh number for various aspect ratios ($Pr = 0.7$).

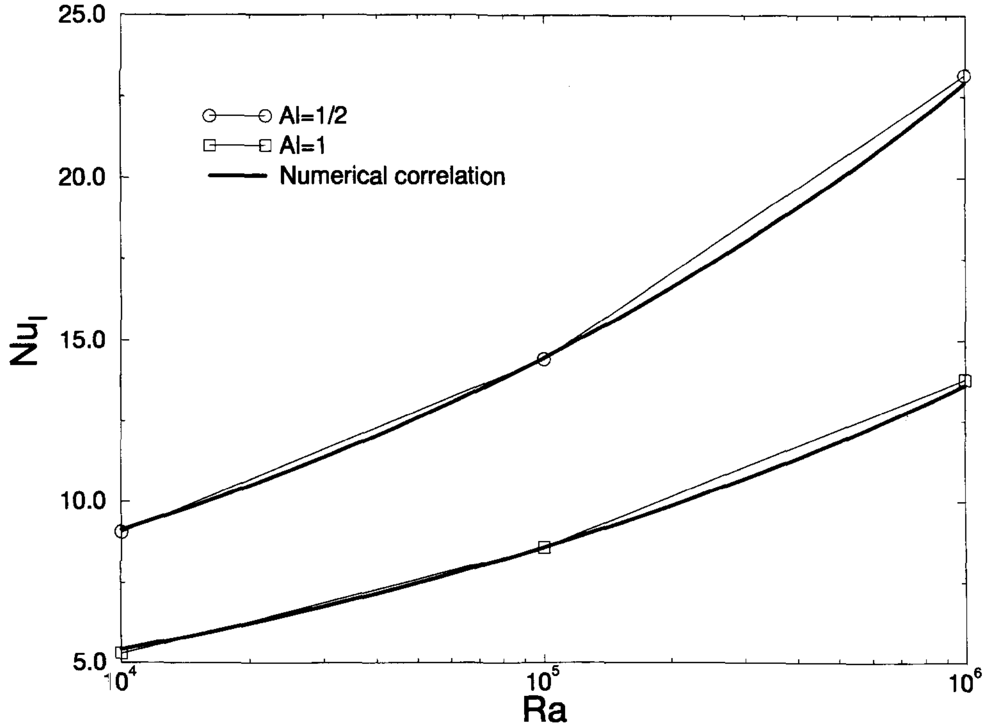

Fig. 17. Lateral Nusselt number vs Rayleigh number and numerical correlation $Nu_l = 0.86Al^{-0.75}Ra^{0.2}$.

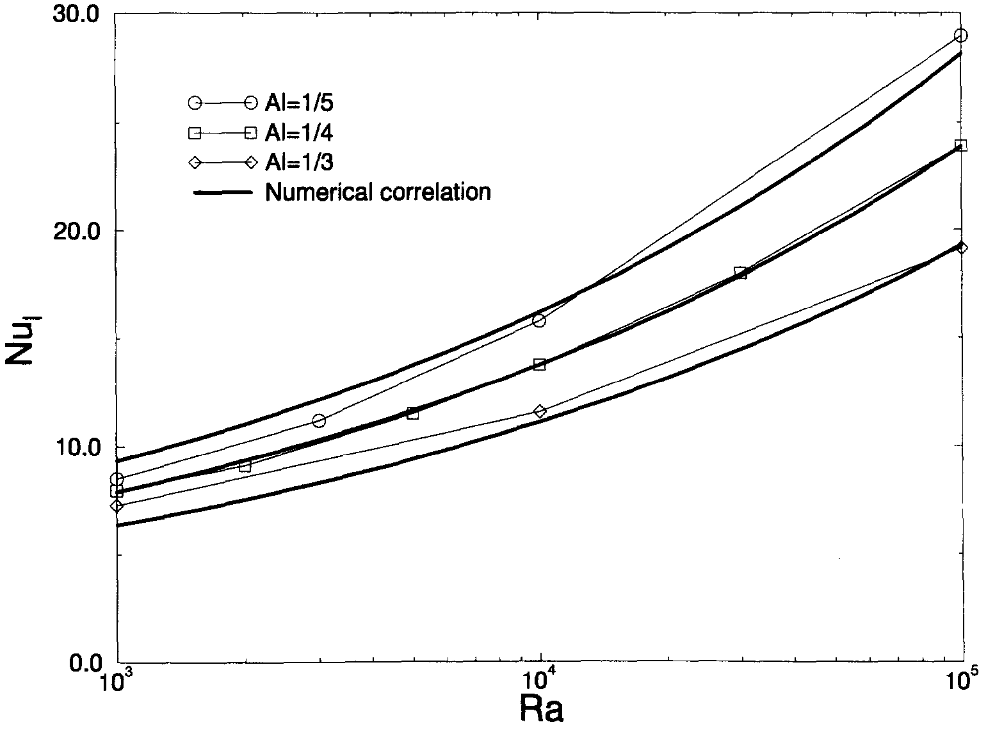

Fig. 18. Lateral Nusselt number vs Rayleigh number and numerical correlation $Nu_l = 0.54Al^{-0.74}Ra^{0.24}$.

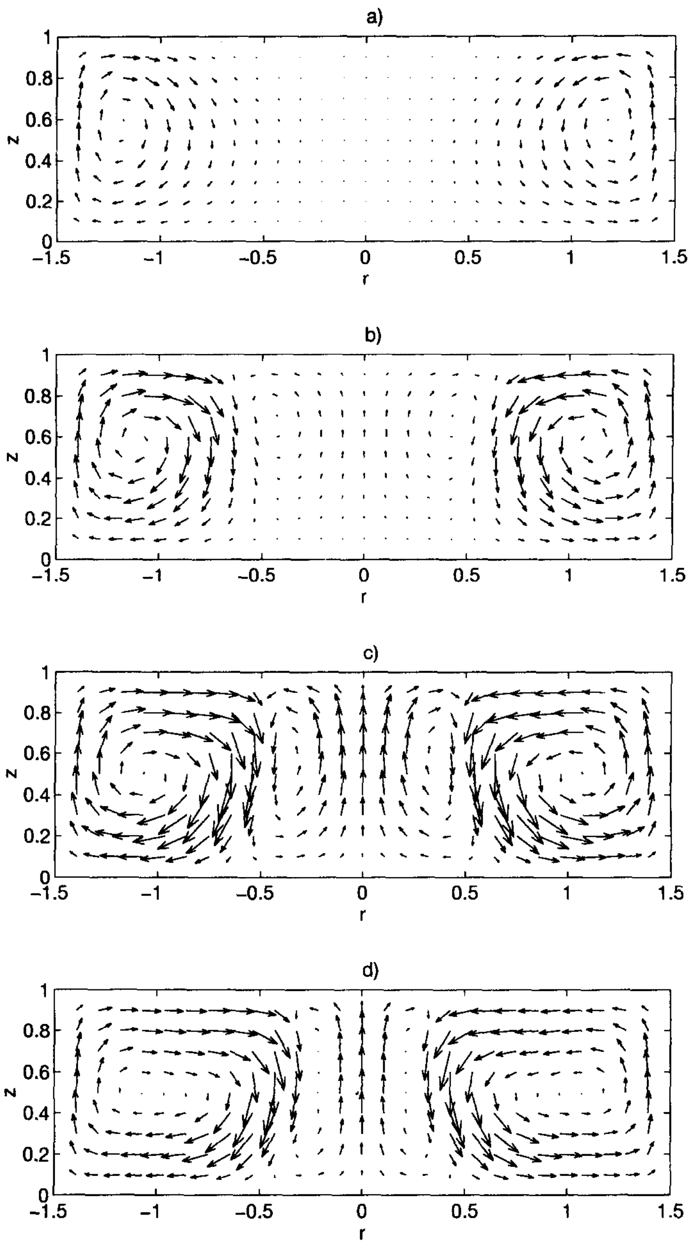

Fig. 19. Transient flow field for $Ra = 10^5$, $Pr = 7$, $Al = 1/3$; (a) $t = 14$, $V_{max} = 0.044$; (b) $t = 21$, $V_{max} = 0.074$; (c) $t = 28$, $V_{max} = 0.125$; (d) $t = 35$, $V_{max} = 0.109$ (the visualizations have the same velocity scale).

when the aspect ratio or the Rayleigh number increases at both the top and lateral surfaces, except for $Al = 1$ and $Al = 2$ where the lateral Nusselt number is little influenced by the aspect ratio and Rayleigh number. The convective heat transfer is more important at the top surface for $1/5 \leqslant Al \leqslant 1/2$. Numerical correlations have been determined for both the top and lateral surfaces. Finally, the maximum velocities appear when $1/2 \leqslant Al \leqslant 1$. In the transient phase of cases where $Al \leqslant 1/3$, a time-limited two-roll flow has been predicted. This phenomenon could result from the combination of a drawing effect of the near side-wall cell and temperature gradient generated vorticity.

Acknowledgement—The computational means used were made available by the Institut de Développement et des Ressources en Informatique Scientifique (I.D.R.I.S.), the C.N.R.S. Computer Center in Orsay, France.

REFERENCES

1. Neumann, G., Three-dimensional numerical simulation of buoyancy-driven convection in vertical cylinders heated from below. *J. Fluid Mech.*, 1990, **214**, 559–578.

2. Figliola, R. S., Convection transitions within a vertical cylinder heated from below. *Phys. Fluids*, 1986, **29**(9), 2028–2031.
3. Guthmann, C., Perrin, B. and Thomé, H., Non-linear behavior of convection in a vertical cylinder cell at high aspect ratio. *J. Phys. France*, 1989, **50**, 2951–2965.
4. Liang, S. F., Vidal, A. and Acrivos, A., Buoyancy-driven convection in cylindrical geometries. *J. Fluid. Mech.*, 1969, **36**(2), 239–256.
5. Huang, D. Y. and Hsieh, S. S., Analysis of natural convection in a cylindrical enclosure. *Numerical Heat Transfer*, 1987, **12**, 121–135.
6. Peaceman, D. W. and Rachford, H. H., Jr. The numerical solution of parabolic and elliptic differential equations. *J. Soc. Indust. Applied Mathematics*, 1955, **3**(1), 28–41.
7. Mitchell, A. R., *Computational Methods in Partial Differential Equations*, John Wiley & Sons, London (1969) pp. 29–31.
8. Roache, P. J., *Computational Fluid Dynamics*, Hermosa Publishers, Albuquerque, New Mexico (1976) p. 93.
9. Schneider, S. and Straub, J., Laminar natural convection in a cylindrical enclosure with different end temperatures. *Int. J. Heat Mass Transfer*, 1992, **35**(2), 545–557.
10. Cotter, M. A. and Charles, M. E., Transient cooling of petroleum by natural convection in cylindrical storage tanks—I. Development of a numerical simulator. *Int. J. Heat Mass Transfer*, 1993, **36**(8), 2165–2174.
11. Ramachandran, N., Gupta, J. P. and Jaluria, Y., Thermal and fluid flow effects during solidification in a rectangular enclosure. *Int. J. Heat Mass Transfer*, 1982, **25**(2), 187–194.
12. Hadjisophocleous, G. V., Sousa, A. C. M. and Venart, J. E. S., Prediction of transient natural convection in enclosures of arbitrary geometry using a nonorthogonal numerical model. *Numerical Heat Transfer*, 1988, **13**, 373–392.